 CMES, vol.16, no.2, pp.83-101, 2006

3D Multi-Material Structural Topology Optimization with the Generalized Cahn-Hilliard Equations

Shiwei Zhou[1] **and Michael Yu Wang**[2]

Abstract: This paper describes a self-mass-conservative Cahn-Hilliard (C-H) model with elastic strain energy (mean compliance) for the optimization of multi-material structure topology. The total free energy of the generalized C-H system can be represented as a Lyapunov functional so that the elastic strain energy, as a part of the total free energy, decreases gradually to attain optimal material distribution. The interface energy relating to phase gradient in the total free energy plays an important role in regularizing the original ill-posed problem by restricting the structure's boundaries. On the other hand, interface coalescence and break-up due to phase separation and grain coarsening result in spontaneous and flexible topology changes. To solve the generalized C-H system with elasticity in 3D, which is described by a set of fourth-order nonlinear parabolic PDEs, we develop a powerful implicit multigrid algorithm and prove non-increasing in total free energy and the convergence. Our results are compared with the results of the well-known SIMP model for single material structural topology in 3D. Furthermore, applications to several well-known 3D examples for multi-material structural topology optimization are presented.

keyword: Structural Topology Optimization, Cahn-Hilliard Equation, Multi-Material, 3D.

1 Introduction

Since the original concept of topology optimization problems was proposed by [Bendsoe and Kikuchi (1988)], many methods have been developed for their various applications. However, especially for structural topology optimization, only a few approaches give examples in three-dimensional conditions, which were reported in [Allaire, Bonnetier, Francfort, and Jouve (1997)] by homogenization method with a topology optimization algorithm, [DeRose and Diaz (2000)] by SIMP alike model with a meshless, wavelet-based scheme, [Allaire, Jouve, and Taoder (2004)] by level set method and [Borrvall and Petersson (2001)] by a regularized intermediate density control scheme. There are also other indirect methods with post-smoothing techniques by geometric reconstruction [Tang and Chang (2001)] or cellular automata [Kita and et al. (2004)]. But a limitation of these schemes comes from the fact that the structures are supposed to be composed of single material. For the optimization of multi-material structural topology in 3D, the existing methods have limited range of applications.

The main condition in multi-material structural topology optimization is to maintain material volume ratio constraints for different material phases. In this paper, we are concerned with the problem of finding the material distribution in a given design domain such that the structure is the stiffest [Bendsoe and Sigmund (2003)]. Obviously, the more materials the structure has, the stronger the structure is. So the process of optimization should be mass-conservative. Traditional methods usually satisfy these constraints with Lagrange multipliers added to the objective function or indirect asymptotic MMA (Method of Moving Asymptotes) scheme [Svanberg (1987)]. But these methods are not self-conservative, just leading to a gradient flow in the norm of L^2.

In this paper, we introduce a self-conservative gradient flow in the norm of H^{-1} for the problem of multi-material structural topology in 3D with a generalized C-H model with elasticity. The prototype of C-H model [Cahn and Hilliard (1958); Cahn (1961)], explaining phase separation and grain coarsening for quenched alloy, is mass-conservative, energy-dissipative and topology-flexible. Such properties are invariable even when disturbing elastic energy is added to the total free energy, which originally only consists of bulk energy and interface energy. Thus the generalized C-H model with elasticity is espe-

[1] Department of Automation and Computer-Aided Engineering,The Chinese University of Hong Kong, Shatin, N.T., Hong Kong, China. E-mail address: swzhou@acae.cuhk.edu.hk

[2] Department of Automation and Computer-Aided Engineering,The Chinese University of Hong Kong, Shatin, N.T., Hong Kong, China. E-mail address: yuwang@acae.cuhk.edu.hk

cially suitable for the topology optimization to minimize the mean compliance (elastic energy) with given materials.

This new model is represented by a set of fourth-order nonlinear parabolic equations, which are really inefficient to be solved by common methods like finite difference and FEM scheme. Here we develop a powerful implicit multigrid algorithm in 3D with mathematical proof of non-increasing total free energy and convergence. We can't prove the dissipation of elastic energy, but from real examples, actually it declines gradually all the time. The simulation for the quadternary C-H system without elasticity in 3D demonstrates this algorithm is fast and correct. Such simulation is pioneer for the C-H model composed of more than three phases in 3D to our best knowledge.

This paper is organized as follows: Section 2 gives a mathematic model for the structural topology optimization and some basic concept about SIMP model. Then Section 3 details the generalized C-H model with elasticity and its numerical implementation by multigrid algorithm is described in Section 4. The proofs of non-increasing total free energy and convergence for this multigrid algorithm are discussed in Appendix A: and Appendix B: respectively. Finally, we give some examples in 3D for the SIMP model and C-H model with/without elasticity in Section 5 and Section 6.

2 Statement of the Problem

Fig. 1 illustrates the structural topology optimization (minimum compliance) problem of a statically loaded linear elastic structure under a single loading case with some Dirichlet boundary conditions on Γ_1 and Neumann boundary conditions on Γ_2 and traction boundary Γ_3. [Bendsoe and Kikuchi (1988); Rozvany (1989)]. The design domain $\Omega \subseteq R^d \quad (d = 2 \text{ or } 3)$ is defined as a $2/3$ dimensional open/bounded set occupied by linear isotropic elastic materials, void material with negligible elasticity tensor, and some fixed non-designable domains. The whole boundary of the design domain Ω consists of three parts: $\Gamma = \partial\Omega = \Gamma_1 \cup \Gamma_2 \cup \Gamma_3$.

External force f and the boundary traction h cause the unique displacement field u in Ω which is the solution of the linear elastic system

$$-\text{div}\,\sigma(u) = f \quad in \quad \chi_\Omega(x) = 1$$

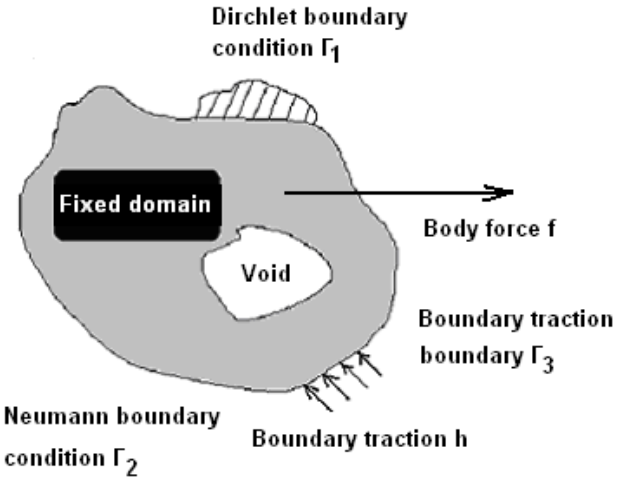

Figure 1 : The problem for the optimization of structural topology in 2D domain

$$\begin{aligned} u &= u_0 \qquad on \quad \Gamma_1 \\ \sigma(u)\cdot n &= 0 \quad on \quad \Gamma_2 \\ \sigma(u)\cdot n &= h \quad on \quad \Gamma_3 \end{aligned} \tag{1}$$

where the strain tensor ε and the stress tensor σ at any point $x \in \Omega$ are given in the usual form as

$$\varepsilon(u) = \frac{1}{2}\left(\nabla u + \nabla u^T\right); \quad \sigma(u) = E\varepsilon(u) \tag{2}$$

with E as the elasticity tensor, u_0 the prescribed displacement on Γ_1, and n the outward normal to the boundary.

In this paper, we consider to use N types of different material phases whose densities or material concentrations at given position x are represented as an order parameter field $c(x) = [c_1, c_2, \ldots, c_N]^T \quad \left(c \in R^N\right)$. It is obvious that the summation of c_i at each position is unity: $\sum_{i=1}^{N} c_i(x) = 1$. The whole material domain of the structure is separated into regions $\Omega = (\Omega_1, \Omega_2, \cdots, \Omega_N)$ for each distinct material phase. This partition leads to

$$\Omega = \bigcup_{i=1}^{N} \Omega_i \quad and \quad \Omega_i \cap \Omega_j = \emptyset, \quad i \neq j \tag{3}$$

The boundary of Ω_i is specified by $\partial\Omega_i$ and the interface between them is given by $\partial\Omega_i \cap \partial\Omega_j$. The material properties in each region are given by the corresponding material phase. For example, the elasticity tensor in Ω is given by $E(x) = E^1$, E^2, or E^N depending on if $x \in \Omega_1$, Ω_2, or Ω_N respectively.

Thus, the "basic" problem of structure optimization is specified with respect to a specific objective function described as the work done by external forces.

$$\begin{aligned} \underset{\Omega}{\text{minmize}}\ & J(u,c) = \int_\Omega f \cdot u d\Omega + \int_{\Gamma_3} h \cdot u d\Gamma \\ s.b.:\ & \int_\Omega c_i d\Omega \le V_i \\ & \frac{1}{2}\int_\Omega \varepsilon_{ij}(u) : E_{ijkl}(c)\,\varepsilon_{kl}(v)\, d\Omega \\ & \quad = \int_\Omega f \cdot v d\Omega \ + \ \int_{\Gamma_3} h \cdot v d\Gamma \\ & \text{for all } v \in U_{ad} \end{aligned} \tag{4}$$

where ':' representing the second order tensor operator, V_i is the limit on the amount of each material phase in terms of its maximum admissible volume and v is the virtual displacement in the kinematically admissible displacement fields:

$$U_{ad} = \left\{ u :\ u \in H^1(\Omega);\ u = \ u_0 \text{ on } \Gamma_1 \right\} \tag{5}$$

The goal of optimization is to find a minimizer Ω such that the design has the following characteristic functions [Bendsoe and Kikuchi (1988); Bendsoe and Sigmund (1999); Bendsoe and Sigmund (2003)]:

$$\begin{aligned} & \chi_i(x) :\ \Omega_i \to \{0,\ 1\} \\ & \quad \textit{such that} \quad \chi_i(x) = \begin{cases} 1 \text{ for } x \in \Omega_i \\ 0 \text{ for } x \in \Omega \backslash \Omega_i \end{cases} \end{aligned} \tag{6}$$

with the domain partition conditions in Eq. (3) satisfied. The basic optimization problem as stated is known to be ill-posed as it involves the "free-discontinuities" of the boundaries $\partial\Omega_i$ of Ω_i [Cheng and Olhoff (1981)].

2.1 The SIMP model

Here we only discuss the SIMP model for structure with single material. If the design domain Ω is discretized into mutually disjoint brick elements $\Theta_i, \quad i = 1, \cdots, N_e$, where N_e is the number of elements, according to elastic theory, the objective function in Eq. (4) is equal to:

$$\begin{aligned} \underset{\Omega}{\text{minimize}}\quad & J(u,c) = U : KU = \sum_{i=1}^{N_e} u_e : K_e u_e \\ s.b.:\ & \int_\Omega c d\Omega \le V \\ & c - c_{\min} = 0 \\ & 1 - c = 0 \end{aligned} \tag{7}$$

where U is the global displacement derived from $f = KU$ with external force f and global stiffness matrix $K = \sum_{i=1}^{N_e} c^p K_e$. The element displacement u_e can be extracted from U. Here we use 1 and $c_{min} \ll 1$ to represent solid and void material respectively for the design variables. SIMP method proposes a model with a penalization factor p for the element stiffness matrix:

$$K_e = c^p K_0, \quad p \ge 3 \tag{8}$$

where K_0 is a constant matrix relating to the element geometry. In all the following examples both for SIMP and C-H mdoel, the derivation of K_0 is similarly based on standard brick element.

We extend the famous SIMP model from 2D to 3D based on Sigmund's 99 line code in Matlab [Sigmund (2001)]. It uses filter technique to average shape sensitivity among neighboring elements and OC algorithm to update the design variables, all of them are encoded in a short 177 line Matlab program.

3 Structural Topology Optimization using C-H Model

When liquid alloy is quenched, phase separation (spinodal decomposition) takes places. Such phenomena can be successfully explained by C-H model in binary [Cahn and Hilliard (1958); Cahn (1961)] and multiphase [Defontaine (1967); Eyre (1993)] conditions. As the theoretical studying and numerical simulation for the classical C-H model seem now to have reached maturity, the interest tends to shift toward its derivative models. For example, how about the shape and topology change for different phases during phase separation and grain coarsening if considering elastic role, which is the type of setting discussed in this paper.

Many people have done this work about C-H model with elasticity [Garcke (2000); Garcke, Nestler, and Stoth (1999); Garcke, Nestler, and Stinner (2004); Garcke, Rumpf, and Weikard (2001); Leo, Lowengrub, and Jou (1998); Fratzl, Penrose, and Lebowitz (1999); Nabarro, Cress, and Kotschy (1996)]. But they evaluated elastic effect just in microscopic scale by assuming the strains come from lattice deformation caused by atom migration and lattice reconstruction. Based on a sharp interface model in [Eshelby (1957)], they introduced a kind

of elastic energy:

$$W(c,\varepsilon)=\frac{1}{2}\int_{\Omega}\left(\varepsilon_{ij}(u)-\varepsilon^{*}_{ij}(c)\right):E_{ijkl}\left(\varepsilon_{kl}(u)-\varepsilon^{*}_{kl}(c)\right) \tag{9}$$

where $\varepsilon^{*}(c)$ is interpolated according to Vegard's law:

$$\varepsilon^{*}(c)=\sum_{i=1}^{N}c_i\varepsilon^{*}(c_i) \tag{10}$$

where $\varepsilon^{*}(c_i)$ is "intrinsic strain" or "spontaneous strain", defined as the strain tensors when the material is made up of pure component of c_i and is unstrained.

It is reasonable for such assumption of elasticity for alloy solidification. Microscopic elastic energy plays a dominant role in phase separation and grain coarsening leading to irregular phase morphology and variation of solidification speed. But for imaginary problem of structural topology optimization with C-H model, such real elasticity is usually too small to reflect large phase metamorphosis both in shape and topology. In this new scenario, all strains are definitely caused by external body force f and boundary traction h. Then, as discussed in Section 2, the new elastic energy is defined as the work done by external forces:

$$\begin{aligned}W^{*}(c,\varepsilon)&=\int_{\Omega}f\cdot u d\Omega+\int_{\Gamma_3}h\cdot u d\Gamma\\&=\frac{1}{2}\int_{\Omega}\varepsilon_{ij}(u):E_{ijkl}(c)\varepsilon_{kl}(u)d\Omega\end{aligned} \tag{11}$$

Based on the elastic energy in Eq. (11) and the C-H theory, it is straightforward to transport these ideas into a computational model for the continuous topology optimization. The modified C-H model relies on the minimization of the following generalized total "free-energy" functional:

$$\Psi(c,\nabla c,\varepsilon)=\int_{\Omega}\{F(c)+\frac{1}{2}\nabla c:\Gamma_{\varepsilon}\nabla c+\eta W^{*}(c,\varepsilon)\}d\Omega \tag{12}$$

where Γ_{ε} is a constant semidefinite matrix relating to interface thickness, η is a weighting constant. The well function function F usually has several minima corresponding to distinct phase. The first variation of the free energy is the chemical potential:

$$\mu_k=\frac{\partial F(c)}{\partial c_k}-(\nabla\cdot\Gamma_{\varepsilon}\nabla c)_k+\eta\frac{\partial W^{*}(c,\varepsilon)}{\partial c_k} \tag{13}$$

where $k=1,\cdots,N$.

By regarding the negative chemical potential as the thermodynamic forces like the derivation of classic C-H in [Cahn and Hilliard (1958); Elliott (1989)], we get the generalized C-H equations with elasticity:

$$\frac{\partial c_k(x,t)}{\partial t}=\nabla\cdot(M(c)\nabla\mu_k)\quad k=1,\cdots,N \tag{14}$$

and Neumann boundary conditions

$$\frac{\partial c}{\partial n}=\frac{\partial\mu}{\partial n}=0\quad x\in\partial\Omega \tag{15}$$

For simplicity, it assumes the system is in quasi-static equilibrium state [Garcke (2000)]. In other words, the elastic deformation is much quicker than phase changes:

$$\nabla\cdot\frac{\partial W^{*}}{\partial\varepsilon}=0 \tag{16}$$

The corresponding topology optimization problem is then transferred to find the solution of c^{*} for the Eqs. (14)-(16).

These two types of elastic energy are analogical in nature and the proof of resolution existence/uniqueness, mass-conservative and energy dissipative for the generalized C-H with elastic energy in Eq. (9) by [Garcke (2000)] is still valid for its derivative form [Zhou and Wang (2005)].

4 Multigrid Algorithm for the Generalized C-H Equations in 3D

Eqs. (14) are a set of fourth-order nonlinear parabolic equations and rigorous to be solved by traditional schemes like FEM and finite difference. Here we develop a powerful multigird algorithm in 3D with proof of non-increasing total free energy and convergence. This algorithm was first proposed for classic C-H model without elasticity by [Kim (2002); Kim, Kang, and Lowengrub (2004b); Kim, Kang, and Lowengrub (2004a)] and more details should be found in relating references.

4.1 Generalized quadternary C-H model with elasticity

We first expand the Eqs. (14) for a system composed of four phases. Considering unit summation for the mass concentration, we get

$$\begin{cases}\frac{\partial c}{\partial t}=\nabla\cdot(M(c)\nabla\mu)\\ \mu=f(c)-\hat{\Gamma}_{\varepsilon}\Delta c+w(c,\varepsilon)\end{cases} \tag{17}$$

where

$$
\begin{aligned}
c &= \begin{pmatrix} \alpha \\ \beta \\ \gamma \end{pmatrix}, \quad \mu = \begin{pmatrix} \xi \\ \zeta \\ \psi \end{pmatrix}, \\
\hat{\Gamma}_\varepsilon &= \begin{pmatrix} \varepsilon_1^2+\varepsilon_4^2 & \varepsilon_4^2 & \varepsilon_4^2 \\ \varepsilon_4^2 & \varepsilon_2^2+\varepsilon_4^2 & \varepsilon_4^2 \\ \varepsilon_4^2 & \varepsilon_4^2 & \varepsilon_3^2+\varepsilon_4^2 \end{pmatrix} \\
f(c) &= \begin{pmatrix} \frac{\partial F}{\partial \alpha} \\ \frac{\partial F}{\partial \beta} \\ \frac{\partial F}{\partial \gamma} \end{pmatrix}, \quad w(c,\varepsilon) = \eta \begin{pmatrix} \frac{\partial W^*}{\partial \alpha} \\ \frac{\partial W^*}{\partial \beta} \\ \frac{\partial W^*}{\partial \gamma} \end{pmatrix}
\end{aligned} \tag{18}
$$

The bulk energy is defined as

$$
\begin{aligned}
F(c) = \kappa[&\alpha^2(\beta^2+\gamma^2+\nu^2)+\beta^2(\gamma^2+\nu^2) \\
&+\gamma^2\nu^2+\alpha^2\beta^2(\gamma^2+\nu^2)+\beta^2\gamma^2\nu^2]
\end{aligned} \tag{19}
$$

where $\nu = (1-\alpha-\beta-\gamma)$ is the fourth phase. κ is a parameter to control the well function in Eq. (19). $\hat{\Gamma}_\varepsilon$ is a derivation from $\Gamma_\varepsilon = \begin{bmatrix} e_1\varepsilon_1^2 & e_2\varepsilon_2^2 & e_3\varepsilon_3^2 & e_4\varepsilon_4^2 \end{bmatrix}$, where $e_i, i = 1, \cdots, 4$ are eigenvectors.

Combining Eqs. (17)-(19), we get

$$
\begin{cases}
\frac{\partial \alpha}{\partial t} = \nabla \cdot (M(c)\nabla \xi) \\
\frac{\partial \beta}{\partial t} = \nabla \cdot (M(c)\nabla \zeta) \\
\frac{\partial \gamma}{\partial t} = \nabla \cdot (M(c)\nabla \psi)
\end{cases} \tag{20}
$$

where

$$
\begin{cases}
\xi = f_1 - (\varepsilon_1^2+\varepsilon_4^2)\Delta\alpha - \varepsilon_4^2\Delta(\beta+\gamma) + w_1 \\
\zeta = f_2 - (\varepsilon_2^2+\varepsilon_4^2)\Delta\beta - \varepsilon_4^2\Delta(\alpha+\gamma) + w_2 \\
\psi = f_3 - (\varepsilon_3^2+\varepsilon_4^2)\Delta\gamma - \varepsilon_4^2\Delta(\alpha+\beta) + w_3
\end{cases} \tag{21}
$$

Here, $w(c)$ is the sensitivity of the elastic strain energy of the structure with respect to the phase concentration c, which is given by using the adjoint method [Bendsoe and Sigmund (2003)], for example, for $c_1 = \alpha$,

$$
w_1 = \eta \frac{\partial W^*}{\partial c_1} = -\eta p c_1^{p-1} u : E_1 u \tag{22}
$$

where $p > 1$

4.2 Approximation of nonlinear bulk function derivative

Discretize the first items in Eqs. (20) and (21) by Crank-Nicholson scheme:

$$
\frac{\alpha_{ijk}^{n+1} - \alpha_{ijk}^n}{\tau} = \nabla \cdot \left[M\left(c_{ijk}^n\right) \nabla \left(\xi_{ijk}^{n+1/2} \right) \right] \tag{23}
$$

$$
\begin{aligned}
\xi_{ijk}^{n+1/2} = &\hat{f}_1\left(c^n, c^{n+1}\right) \\
&- \frac{1}{2}\left(\varepsilon_1^2+\varepsilon_4^2\right)\Delta\left(\alpha_{ijk}^n + \alpha_{ijk}^{n+1}\right) \\
&- \frac{1}{2}\varepsilon_4^2\Delta\left(\beta_{ijk}^n + \beta_{ijk}^{n+1} + \gamma_{ijk}^n + \gamma_{ijk}^{n+1}\right) \\
&+ \frac{1}{2}\left(w_1\left(c_{ijk}^n\right) + w_1\left(c_{ijk}^{n+1}\right)\right)
\end{aligned} \tag{24}
$$

Here we use α_{ijk}^n and α_{ijk}^{n+1} to represent the values before and after one step of iteration. $\alpha_{ijk}^{n+1/2}$ is a functional of α_{ijk}^n and α_{ijk}^{n+1} and is written as $\alpha\left(c^n, c^{n+1}\right)$ sometimes. The rest items in Eqs. (20) and (21) can be discretized similarly as Eqs. (23) and (24), but we omit them here for brief reason. These six equations make up of a linear equation system with six unknowns relating to updated phase concentration c^{n+1} and chemical potential μ^{n+1} . The process of solving these equations is called smoothing operator (relaxation) in multigird algorithm. With similar smoothing operator in standard V_cycle iteration, Kim *et. al.* [Kim (2002); Kim, Kang, and Lowengrub (2004b); Kim, Kang, and Lowengrub (2004a)] successfully get the resolution of traditional C-H model without elasticity in binary and ternary conditions. Our algorithm is an extension of Kim's work, for details about this algorithm, people are advised to read [Kim (2002); Kim, Kang, and Lowengrub (2004b); Kim, Kang, and Lowengrub (2004a)].

How to approximate the highly nonlinear items $\hat{f}(c^n, c^n+1) = (\hat{f}_1, \hat{f}_2, \hat{f}_3)^T$ in the C-H model, which are the first derivative of the bulk function to the design variables, plays an important role for the multigrid algorithm. Traditional scheme is the Crank-Nicholson method by $\hat{f}(c^n, c^{n+1}) = \frac{1}{2}(\hat{f}(c^n) + \hat{f}(c^{n+1}))$. But it can't ensure the total free energy is non-increasing for ternary C-H system [Kim (2002)]. Thus, to avoid the same disadvantage in 3D quadternary C-H system, We propose a new approximation for these items:

$$
\begin{aligned}
\hat{f}_1\left(c^n, c^{n+1}\right) = &f_1\left(c^{n+1}\right) \\
&- \frac{1}{2!}\left[\frac{\partial f_1\left(c^{n+1}\right)}{\partial \alpha}\overline{\alpha} + \frac{\partial f_1\left(c^{n+1}\right)}{\partial \beta}\overline{\beta} + \frac{\partial f_1\left(c^{n+1}\right)}{\partial \gamma}\overline{\gamma}\right] \\
&+ \frac{1}{3!}\frac{\partial^2 f_1\left(c^{n+1}\right)}{\partial \alpha^2}\overline{\alpha}^2 + \frac{1}{3!}\frac{\partial^2 f_1\left(c^{n+1}\right)}{\partial \beta^2}\overline{\beta}^2 \\
&+ \frac{1}{3!}\frac{\partial^2 f_1\left(c^{n+1}\right)}{\partial \gamma^2}\overline{\gamma}^2 + \frac{2}{3!}\frac{\partial^2 f_1\left(c^{n+1}\right)}{\partial \alpha \partial \beta}\overline{\alpha}\overline{\beta}
\end{aligned}
$$

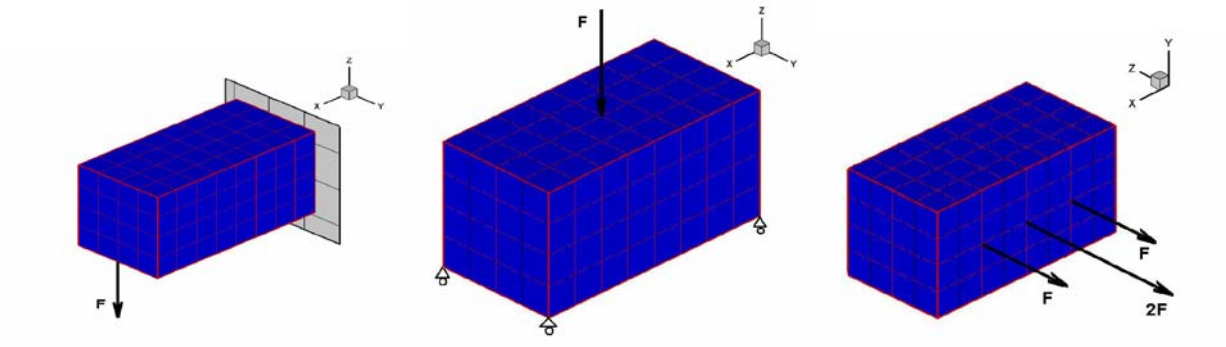

(a) Cantilever beam (b) MBB beam (c) Bridge beam

Figure 2 : The design domains of the three cases

$$+\frac{2}{3!}\frac{\partial^2 f_1\left(c^{n+1}\right)}{\partial\alpha\partial\gamma}\overline{\alpha\gamma}+\frac{2}{3!}\frac{\partial^2 f_1\left(c^{n+1}\right)}{\partial\beta\partial\gamma}\overline{\beta\gamma}$$
$$=f_1\left(c^{n+1}\right)-\frac{1}{2!}\nabla f_1\left(c^{n+1}\right)\cdot\overline{c}$$
$$+\frac{1}{3!}\overline{c}^T H\left(f_1\left(c^{n+1}\right)\right)\cdot\overline{c} \tag{25}$$

where $\overline{\alpha}=\alpha^{n+1}-\alpha^n$, $\overline{\beta}=\beta^{n+1}-\beta^n$ $\overline{\gamma}=\gamma^{n+1}-\gamma^n$, $\overline{c}=c^{n+1}-c^n$ and $H(\cdot)$ is the Hessian matrix.

In the same way, we can derive $\hat{f}_2\left(c^n,c^{n+1}\right)$ and $\hat{f}_3\left(c^n,c^{n+1}\right)$ as

$$\hat{f}_2\left(c^n,c^{n+1}\right)=f_2\left(c^{n+1}\right)$$
$$-\frac{1}{2!}\nabla f_2\left(c^{n+1}\right)\cdot\overline{c}+\frac{1}{3!}\overline{c}^T H\left(f_2\left(c^{n+1}\right)\right)\cdot\overline{c} \tag{26}$$

$$\hat{f}_3\left(c^n,c^{n+1}\right)=f_3\left(c^{n+1}\right)$$
$$-\frac{1}{2!}\nabla f_3\left(c^{n+1}\right)\cdot\overline{c}+\frac{1}{3!}\overline{c}^T H\left(f_3\left(c^{n+1}\right)\right)\cdot\overline{c} \tag{27}$$

Appendix A: proves the total free energy is non-increasing with the above discretization in Eqs. (25-27). They also make sure the multigrid algorithm is convergent, which is proved in Appendix B:.

5 Numerical Examples for SIMP Model:

In this section we illustrate the SIMP model in 3D with three cases extended from standard beams in 2D for the mean compliance optimization problems. The first example is a cantilever beam with a concentrated vertical force $F=1$ at the bottom center of its free vertical surface (Fig. 2a). The second case is a so called MBB beam loaded with a unit concentrated vertical force applied on the center of the top surface (Fig. 2b). The two points at the bottom corner of the left surface are fixed while the two points at the bottom corner of the right surface are simply supported. The last case is a bridge-structure with same boundary conditions as the MBB beam. But it has three evenly located external forces applied on the center line of the bottom surface (in Fig. 2c, the beam is rotated 90^o to display the bottom surface). The middle force is twice larger than the other ones and $F=1$. The design domain for the cantilever beam and the bridge-structure has a 2:1:1 ratio for the length:width:height, but it is 4:1:1 for the MBB beam.

5.1 *Cantilever Beam*

In this example, the mesh is defined as nx = 24; ny = 12; nz = 12 in the direction of x, y and z. The volume ratio is 30% and the initial density for all elements is equal to = 0.3. Penalty factor is p = 3 and filtering radius is r = 1.8. Fig. 3 is the ISO-surface of $c \geq 0.3$ for each iteration (m). From the energy trend in Fig. 4, the SIMP model converges so quickly that only 17 iterations (24 seconds on a computer with Intel(R) Xeron(TM) 3.06 GHz CPU and 1 GB of RAM are needed. The last three snapshots in Fig. 3 are the view of the final structure from different angles.

5.2 *MBB Beam*

For this example, the parameter are the same as the above example except a finer mesh nx = 40; ny = 20; nz = 20 (16,000 cube elements). This example is computed by the same computer with C code to overcome the deficiency of computer memory in Matlab environment. It takes about $35,999.21$ seconds for 32 iterations. This

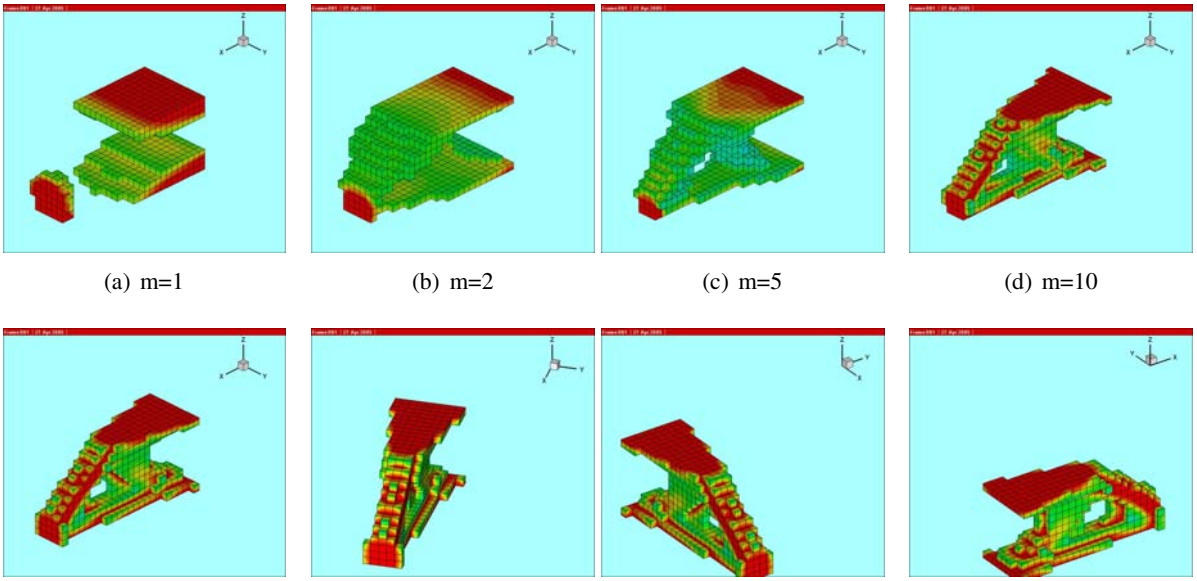

(a) m=1 (b) m=2 (c) m=5 (d) m=10

(e) m=16 (f) angle 1 (g) angle 2 (h) angle 3

Figure 3 : Design process for the cantilever beam

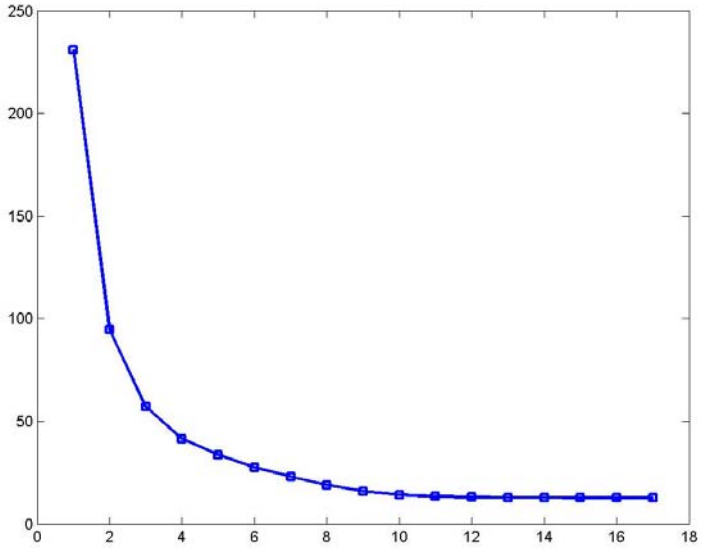

Figure 4 : Energy trend for the cantilever beam

SIMP-based method is much faster than the homogenization based method [Allaire, Bonnetier, Francfort, and Jouve (1997)] which takes one day for 24,000 hexahedral elements on a supercomputer HP9000/755. Fig. 5 gives its design process and Fig. 6 is the enlargement of the final result for clear image.

Fig. 7 illustrates the effect of the penalty factor. The holes on the lateral surfaces disappear as p increases. This is due to the higher penalty factor is able to draw the middle value of density to its two extremes greatly.

5.3 Bridge Beam

This bridge beam example (Fig. 8) is implemented with the same parameters as the cantilever example.

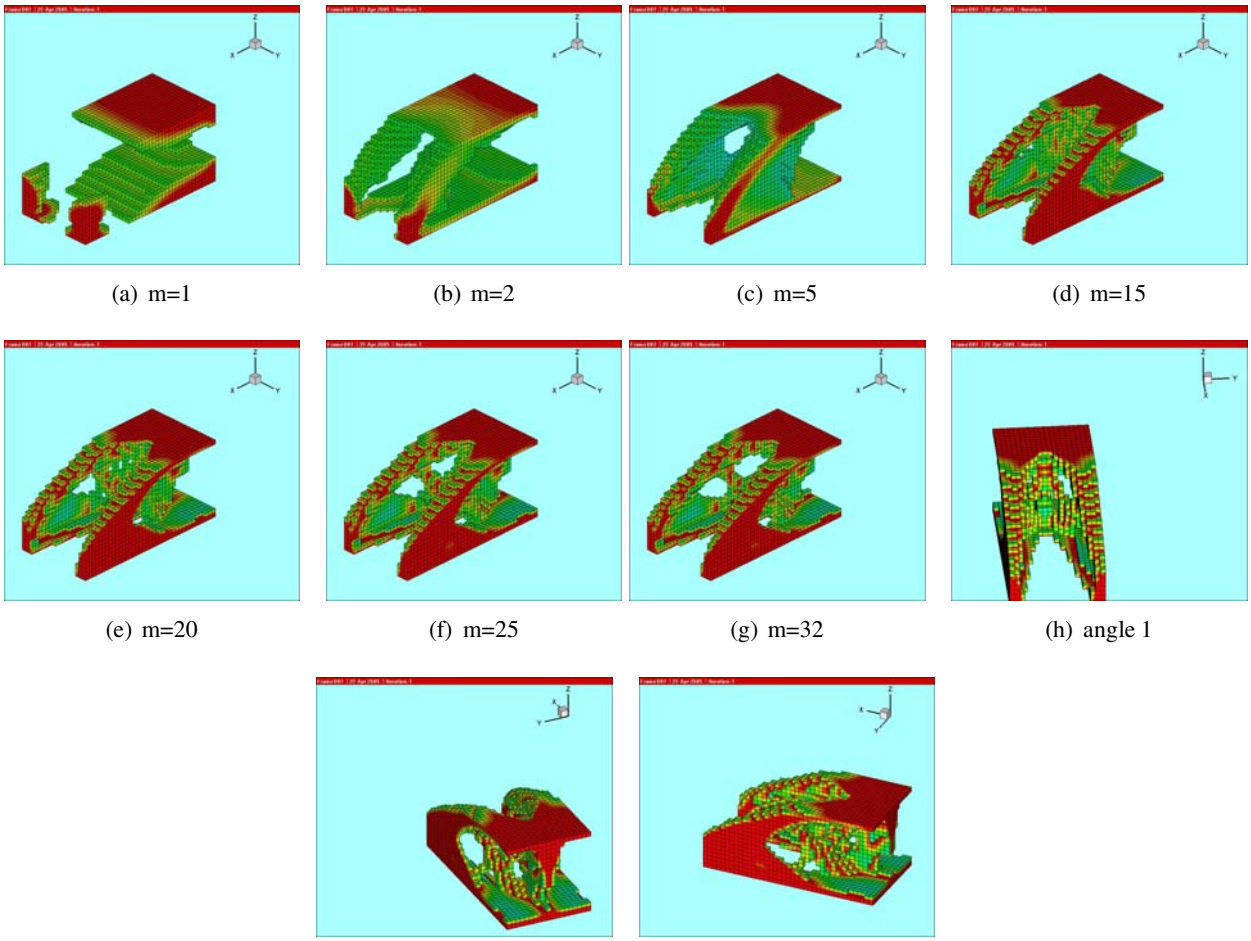

(a) m=1 (b) m=2 (c) m=5 (d) m=15

(e) m=20 (f) m=25 (g) m=32 (h) angle 1

(i) angle 2 (j) angle 3

Figure 5 : Design process for the MBB beam

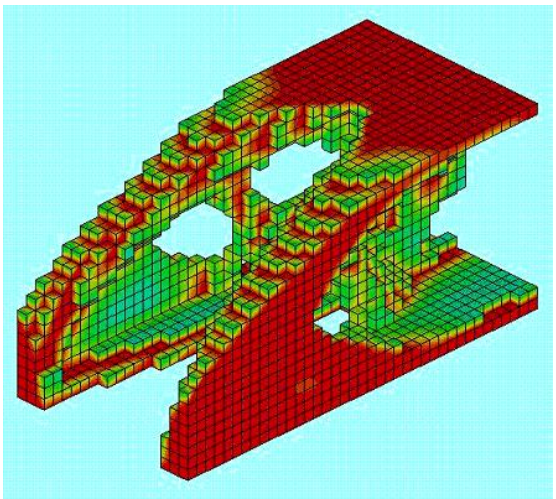

Figure 6 : Enlarged final structure of the MBB beam

6 Numerical Experiments for C-H Model

6.1 Quadraternary C-H Equations

we first illustrate the evolution process for the quadternary C-H equations without elasticity in a cubic domain of $[0,1]\times[0,1]\times[0,1]$ to guarantee the correctness of multigrid algorithm. To our best knowledge at present, no simulation has been made for a C-H system with more than three phases in 3D.

6.1.1 Quadternary C-H Equations with Constant Mobility

The mesh size for this example is $32\times32\times32$ with quadrilateral elements. The volume ratios are 0.15 for the red, 0.2 for the green and 0.25 for the blue. The C-H parameters are all equal to $\varepsilon_1=\varepsilon_2=\varepsilon_3=\varepsilon_4=0.005$. The time step is set as $\tau=0.1h$. Mobility is constant $M=1$. The initial values are nearly homogeneous mate-

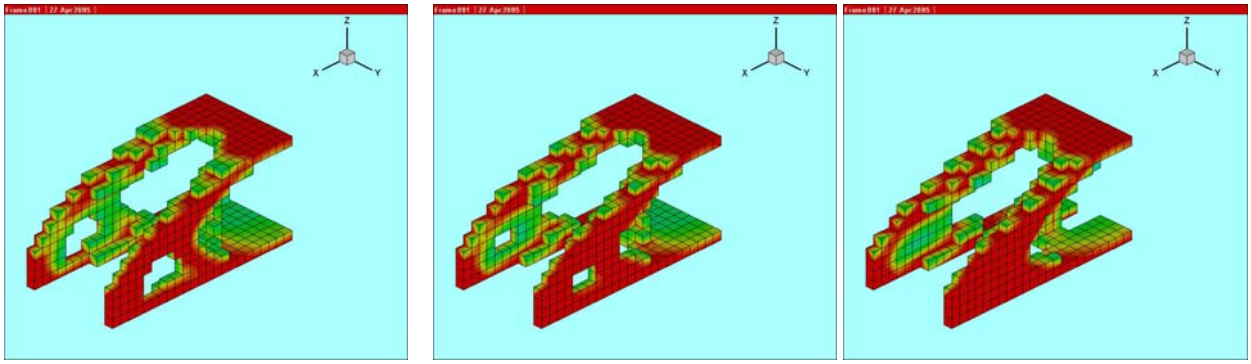

(a) p=3 (b) p=4 (c) p=5

Figure 7 : The final structure of MBB beam with different penalty factor

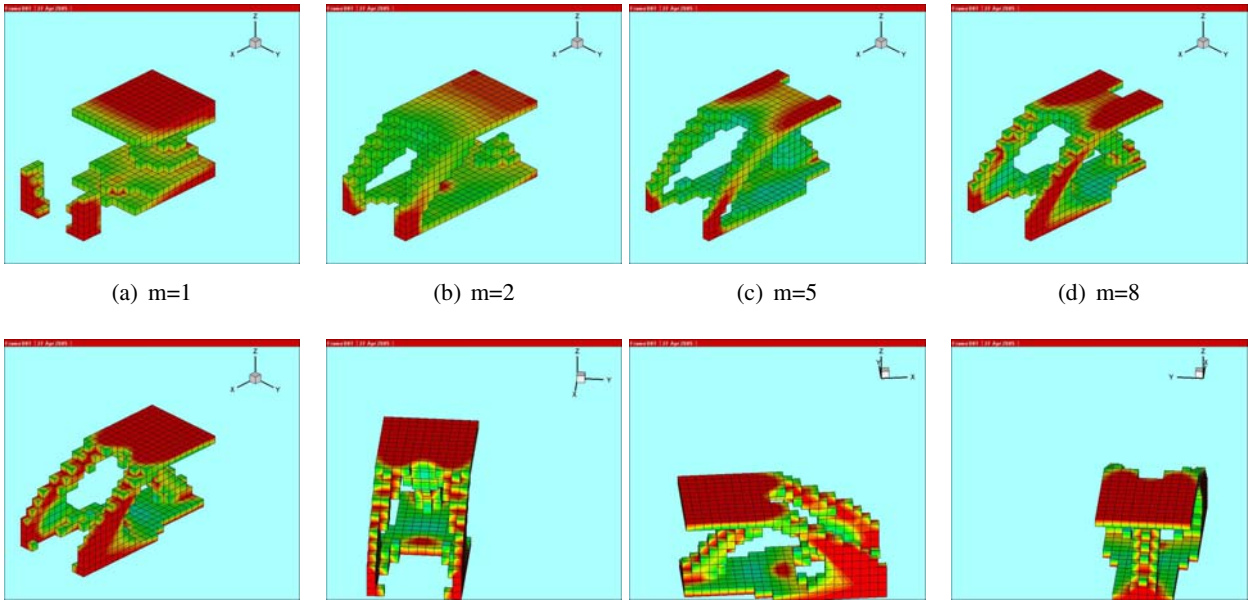

(a) m=1 (b) m=2 (c) m=5 (d) m=8

(e) m=13 (f) angle 1 (g) angle 2 (h) angle 3

Figure 8 : Design process for the bridge beam

rials as

$$\begin{aligned}\alpha(,0) &= 0.15+0.05\cos[2\pi(0.5-rand[0,1])]\\ \beta(,0) &= 0.20+0.05\sin[2\pi(0.5-rand[0,1])]\\ \gamma(,0) &= 0.25+0.05\sin[2\pi(0.5-rand[0,1])]\end{aligned} \tag{28}$$

Fig. 9 lists some external surface snapshots for this evolution. To view the inner structure clearly, we draw the ISO surface with the fourth phase $\nu \geq 0.3$ in Fig. 11.

Fig. 10 illustrates the variation of the interface energy, bulk energy (potential energy) and total free energy in linear and logarithmic coordinates. At the beginning, bulk energy drops sharply and interface energy increases because of phase separation. Then the interface energy drops slowly due to grain size grows up resulting in interface mergence. The total free energy decreases all the time agreeing with the nature of C-H system.

6.1.2 *Quadternary C-H Equations with Varied Mobility*

Here we give another example (Fig. 12) with same parameters as the above example except $M = 0.5 + \alpha(\beta+\gamma+\nu) + \beta(\gamma+\nu) + \gamma\nu$ and $\tau = 0.05h$. Fig. 13 illustrates the inner structure with ISO surface for two snapshots. Fig. 14 compares the energy trend for this example (blue line) with the one with constant mobility (red line). The horizonal axis is nondimensional time. Although the dif-

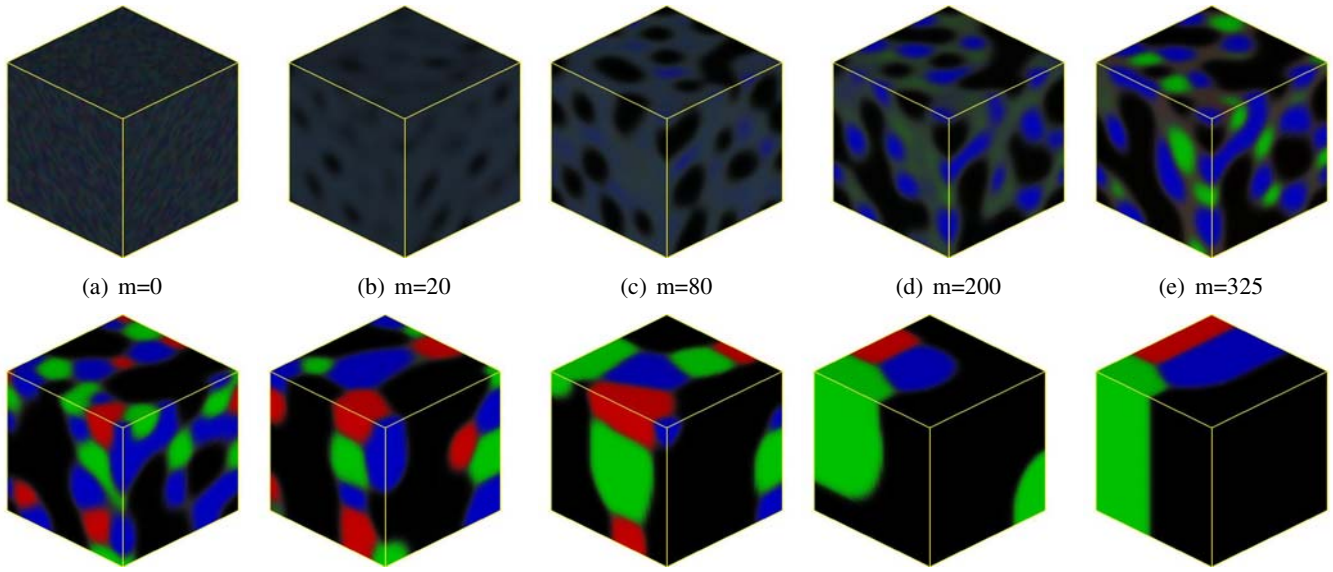

(a) m=0 (b) m=20 (c) m=80 (d) m=200 (e) m=325

(f) m=700 (g) m=1,800 (h) m=4,800 (i) m=17,000 (j) m=79,000

Figure 9 : Surface of quadternary C-H system in 3D with constant mobility

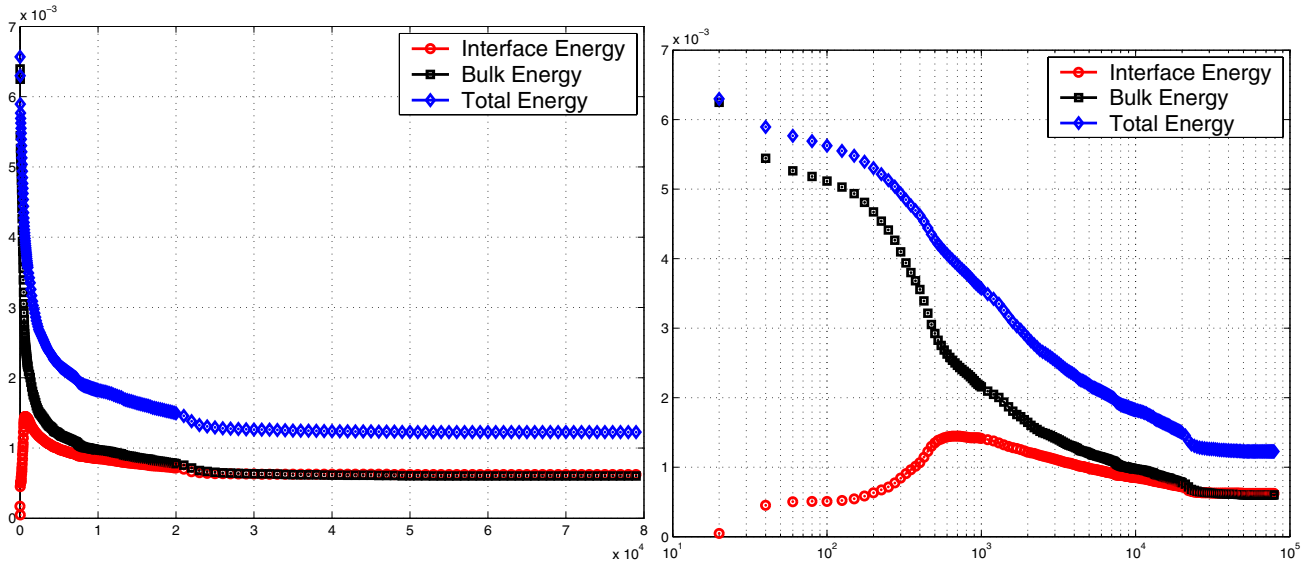

(a) Linear scale (b) Log scale

Figure 10 : Energy trend for quadternary C-H system in 3D with constant mobility

ference of these two curves is small, the example with varied mobility takes much longer time to converge to the final equilibrium state.

6.2 The Optimization of Single Material Structural Topology

In this section, we want to compare the results by SIMP model with the ones by C-H model. As we have developed the codes for ternary C-H system with elasticity for the beams with two materials, we just make use of this program for single material structure by choosing two hard materials (phases) with same stiffness tensor. The stiffness tensor for the rest phase is negligible to represent void. It should be noted the mesh for multigrid is twice finer than the one for FEM to save computing time for all topology optimization examples by C-H model.

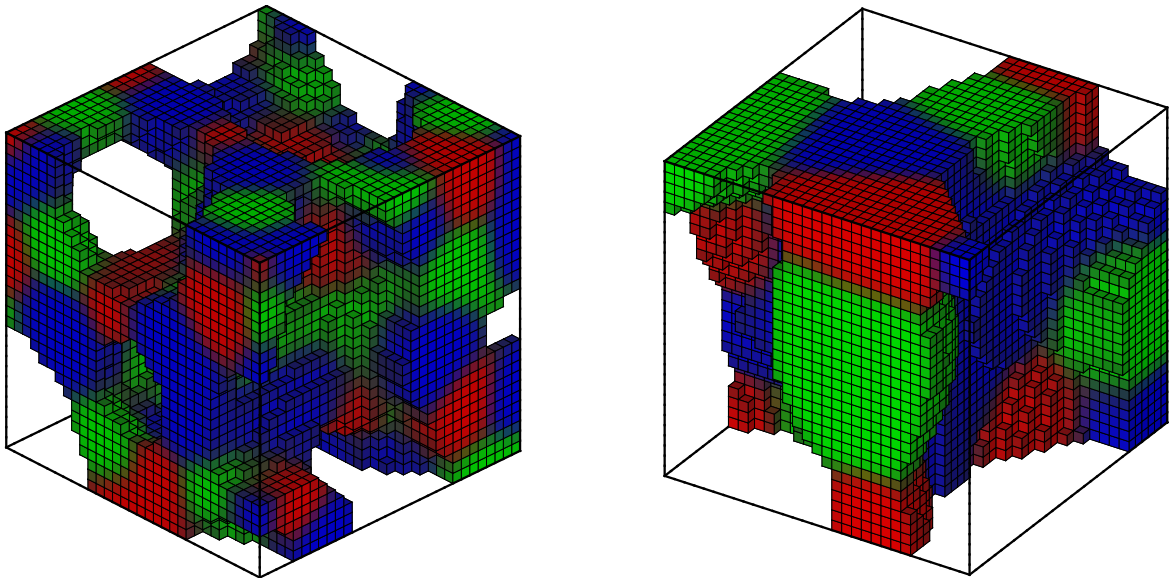

(a) m=700 (b) m=4,800

Figure 11 : ISO surface for quadternary C-H system in 3D with constant mobility

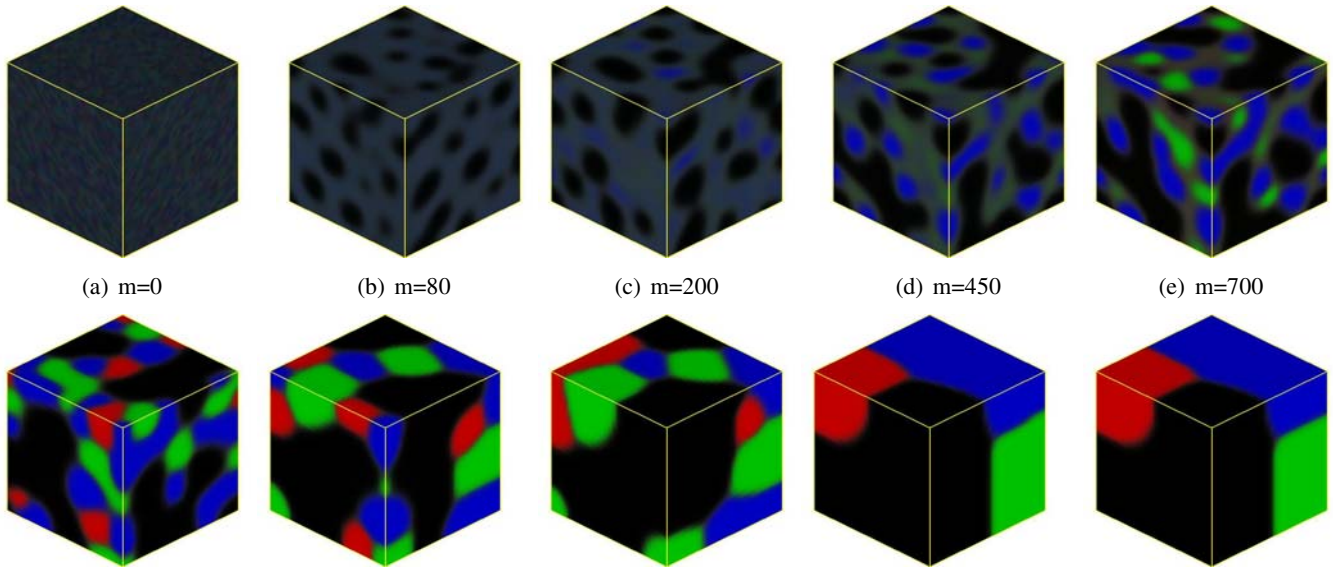

(a) m=0 (b) m=80 (c) m=200 (d) m=450 (e) m=700

(f) m=1,800 (g) m=8,800 (h) m=17,000 (i) m=148,000 (j) m=280,000

Figure 12 : Surface of quadternary C-H system in 3D with varied mobility

6.2.1 MBB Example

The stiffness tensor of the solid material (two phases) is 1 without unit. To avoid computing singularity, we set the stiffness tensor for the void material as 0.001 other than 0 in all examples. The volume ratio for solid material is equal to 0.4. Parameters of the C-H system are set with $\varepsilon_1 = \varepsilon_2 = \varepsilon_3 = 0.01$ and $\eta = 0.025$. A practical time step for the multigrid algorithm is taken as $\tau = 0.01h$ with $32 \times 16 \times 16$ quadrilateral elements. The initial condition for each phase at each element vibrates smally around the volume ratios. Fig. 15 demonstrates the design process. Because of geometry symmetry, only the left part of the MBB beam is designed.

Fig. 16 compared the result by SIMP model with the one by C-H model for MBB beam. The two examples are computed with same volume ration, penalty factor and mesh grid. From the similar results with these two models, it is obvious the C-H model for topology optimiza-

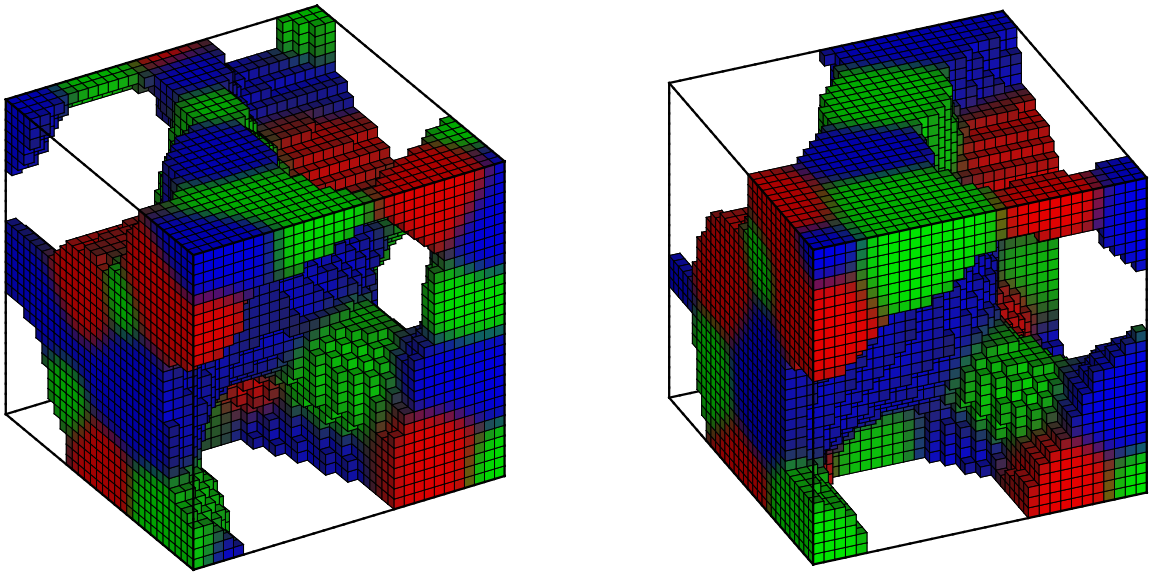

(a) m=4,800 (b) m=8,800

Figure 13 : ISO surface for quadternary C-H system in 3D with varied mobility

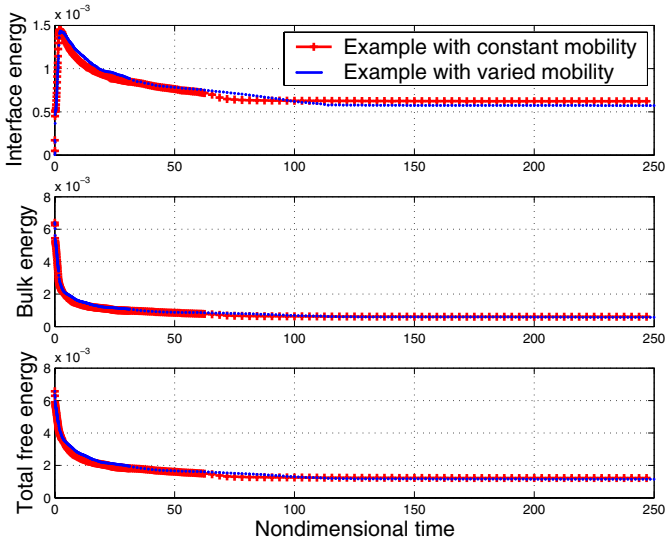

Figure 14 : The energy difference between the example with constant mobility and the one with varied mobility

tion is correct at least for the single material structure.

6.3 *The Optimization of Structural Topology in 3D with Ternary Phases*

Here we consider the optimization of two-material (three phases) structural topology for the same cases as the above section.

6.3.1 *Cantilever Beam*

The mesh size for this example is $32 \times 16 \times 16$ with quadrilateral elements. The volume rations for the hard material (green color, $E = 2$) and soft material (red color, $E = 1$) are 0.2. The C-H parameters are all equal to $\varepsilon_1 = \varepsilon_2 = \varepsilon_3 = 0.01$. Time step is set as $\tau = 0.002h$. Fig. 17 includes some snapshots of ISO-surface with $\gamma \geq 0.5$ for this example.

6.3.2 *MBB Beam*

The parameters for this example are the same as the cantilever example in Fig. 17. Fig. 18 demonstrates the design process for this example.

6.4 *The Optimization of Structural Topology in 3D with Quadternary Phases*

For a structure composed of three solid materials and one void, it is possible to be modeled by the quadternary C-H system for its topology optimization.

6.4.1 *MBB Beam*

The volume rations are 0.1, 0.15 and 0.15 for three solid materials with stiffness tensor 1, 2 and 4 respectively. The mesh gird for multigrid is $32 \times 16 \times 16$, which is double finer than the one of $16 \times 8 \times 8$ for FEM. Each mesh discretized the design domain into a set of identical cube elements. The C-H parameters are all equal

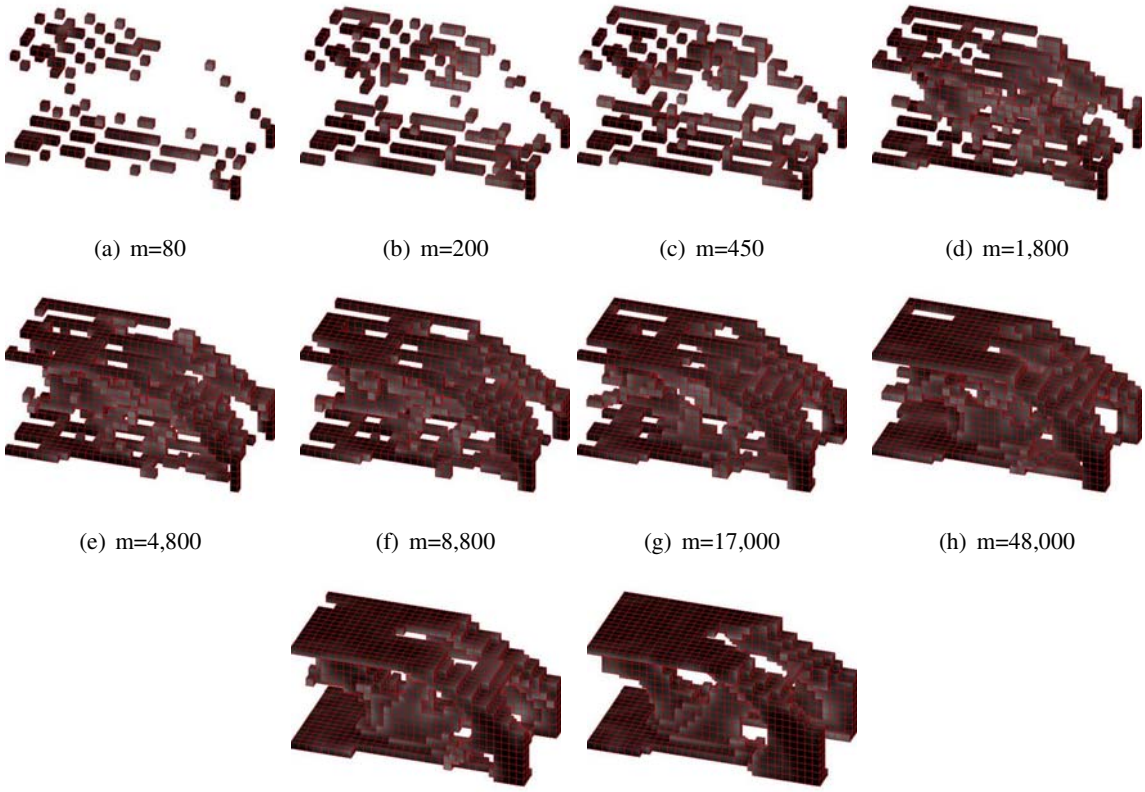

(a) m=80 (b) m=200 (c) m=450 (d) m=1,800

(e) m=4,800 (f) m=8,800 (g) m=17,000 (h) m=48,000

(i) m=148,000 (j) m=280,000

Figure 15 : The optimization of single material structural topology by C-H model (MBB beam)

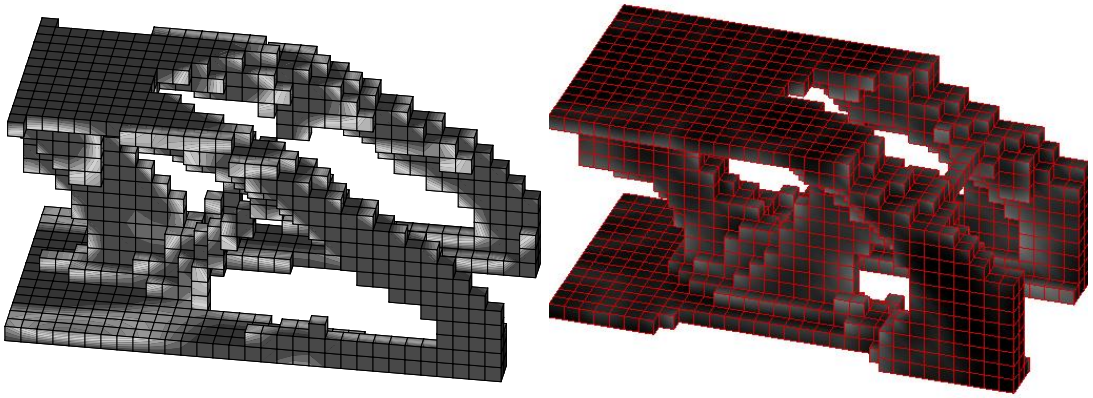

(a) SIMP model (b) C-H model

Figure 16 : The result by C-H model compared with the result by SIMP model (MBB beam)

to $\varepsilon_1 = \varepsilon_2 = \varepsilon_3 = \varepsilon_4 = 0.01$ and time step is set as $\tau = 0.002h$. The elastic parameter is equal to $\eta = 0.015$ for this example. Fig. (19 a) displays the right half of the optimized structure. It has to note the final result is not strictly accurate due to the FEM is computed on a coarser grid for saving time. But from the energy trend in Fig. (19 b), both total free energy and elastic energy drops gradually indicating such FEM approximation is reasonable.

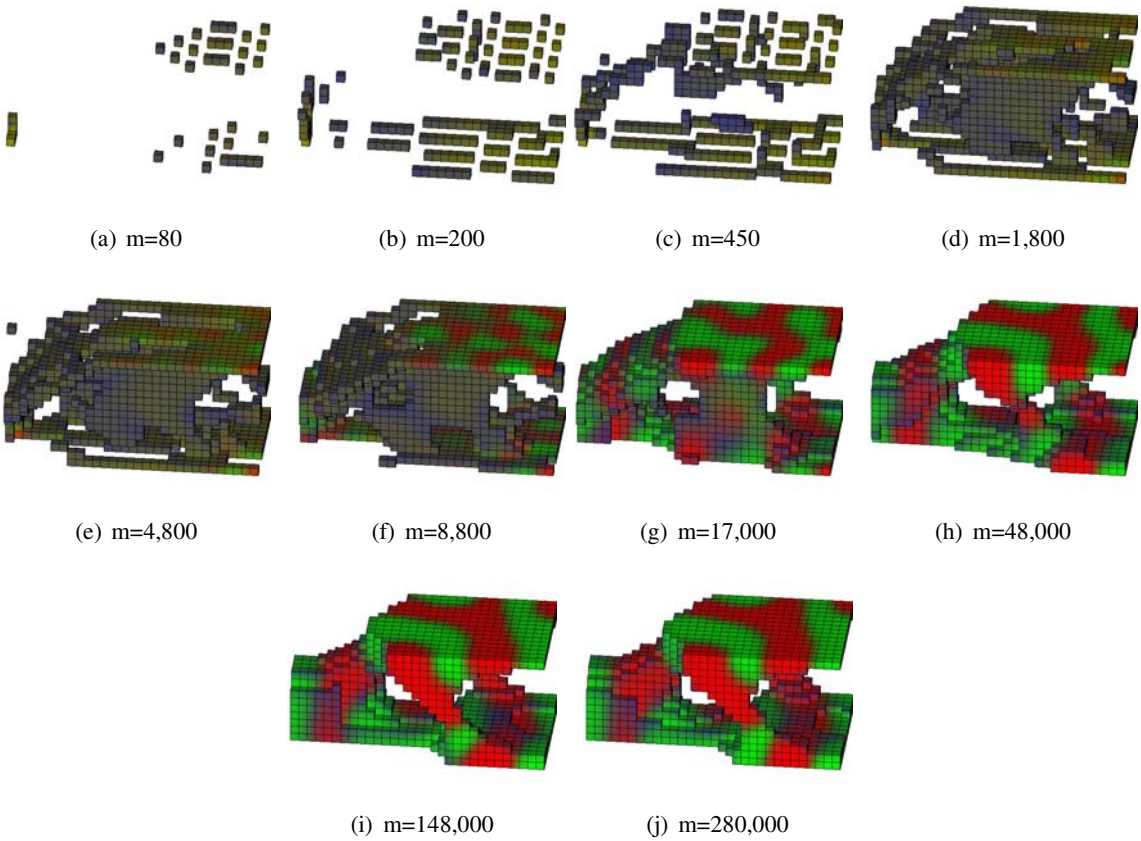

(a) m=80 (b) m=200 (c) m=450 (d) m=1,800

(e) m=4,800 (f) m=8,800 (g) m=17,000 (h) m=48,000

(i) m=148,000 (j) m=280,000

Figure 17 : The optimization of two material structural topology by C-H model (cantilever beam)

References

Allaire, G.; Bonnetier, E.; Francfort, G.; Jouve, F. (1997): Shape optimization by the homogenization method. *Numerische Mathematic*, vol. 76, pp. 27–68.

Allaire, G.; Jouve, F.; Taoder, A.-M. (2004): Structural optimization using sensitivity analysis and a level-set method. *J. Computational Physics*, vol. 194, pp. 363–393.

Bendsoe, M. P.; Kikuchi, N. (1988): Generating optimal topologies in structural design using a homogenisation method. *Computer Methods in Applied Mechanics and Engineering*, vol. 71, pp. 197–224.

Bendsoe, M. P.; Sigmund, O. (1999): Material interpolations in topology optimization. *Archive of Applied Mechanics*, vol. 69, pp. 635–654.

Bendsoe, M. P.; Sigmund, O. (2003): *Topology Optimization: Theory, Methods and Applications*. Springer-Verlag.

Borrvall, T.; Petersson, J. (2001): Large-scale topology optimization in 3d using parallel computing. *Comput. Methods Appl. Mech. Eng.*, vol. 190, pp. 6201–6229.

Cahn, J.; Hilliard, J. E. (1958): Free energy of a nonuniform system. i. interfacial free energy. *Journal of Chemical Physics*, vol. 28, no. 1, pp. 258–267.

Cahn, J. W. (1961): On spinodal decomposition. *Acta Metall.*, vol. 9, pp. 795–801.

Cheng, K. T.; Olhoff, N. (1981): An investigation concerning optimal design of solid elastic plates. *International Journal of Solids and Structures*, vol. 17, pp. 305–323.

Defontaine, D. (1967): *A computer simulation of the evolution of coherent composition variations in solid solutions*. PhD thesis, Northwestern University, 1967.

DeRose, G. C. A.; Diaz, A. R. (2000): Solving three-dimensional layout optimization problems using fixed

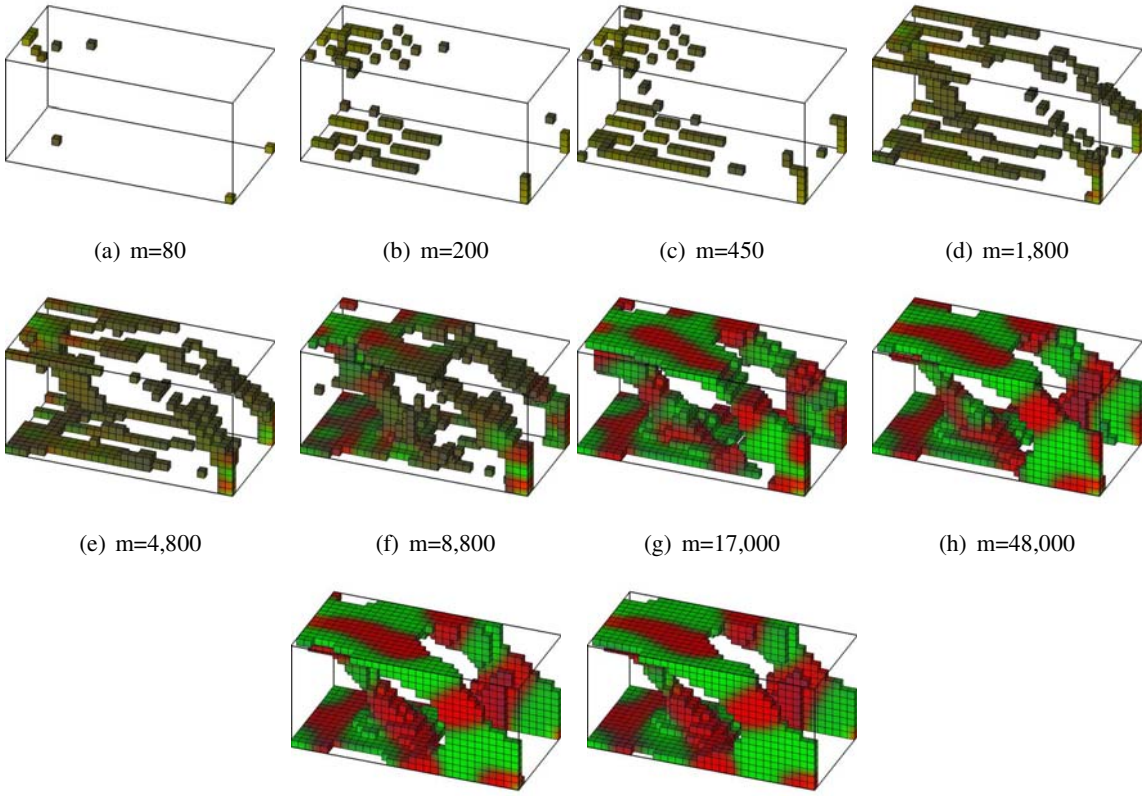

(a) m=80 (b) m=200 (c) m=450 (d) m=1,800

(e) m=4,800 (f) m=8,800 (g) m=17,000 (h) m=48,000

(i) m=148,000 (j) m=280,000

Figure 18 : The optimization of two material structural topology by C-H model (MBB beam)

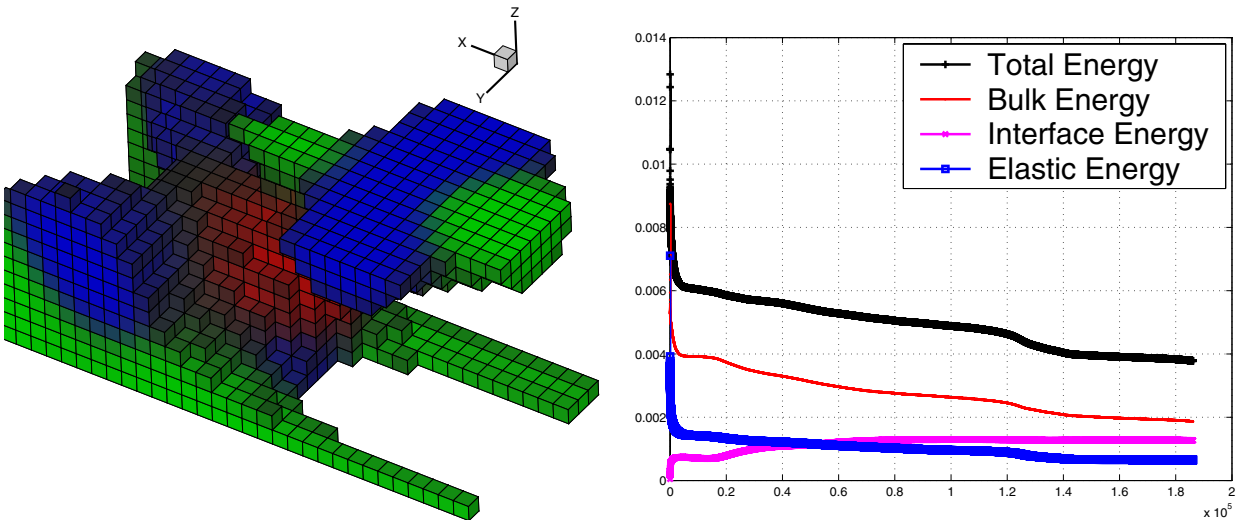

(a) The optimal topology for a MBB beam composed four phases

(b) Energy trend for the MBB beam composed four phases

Figure 19 : The optimization of three material structural topology by C-H model (MBB beam)

scale wavelets. *Computational Mechanics*, vol. 25, pp. 274–285.

Kita, E.; Saito, H.; Kobayashi, T.; Xie, Y.M. (2004): 3d topology optimizatin using cellular automata. *High*

Performance Structures and Materials II, vol. 193, no. C. A. Brebbia and W. P. De Wilde, pp. 511–543.

Elliott, C. M. (1989): The cahn-hilliard model for the kinetics of phase separation. In Rodrigues, J. F.(Ed): *Mathematical models for phase change problems, international series of numerical mathematics*, volume 88, pp. 405–471, Birkhauser Verlag Basel.

Eshelby, J. (1957): The determination of the elastic field of an ellipsoidal inclusion and related problems. *Proc. Roy. Soc.*, vol. A241, pp. 376–396.

Eyre, D. (1993): Systems of cahn-hilliard equations. *SIAM J. Appl. Math.*, vol. 53, no. 6, pp. 1686–1712.

Fratzl, P.; Penrose, O.; Lebowitz, J. L. (1999): Modeling of phase separation in alloys with coherent elastic misfit. *Journal of Statistical Physics*, vol. 95, no. 5/6, pp. 1429–1503.

Garcke, H. (2000): *On mathematical models for phase separation in elastically stressed solids*. PhD thesis, University Bonn, 2000.

Garcke, H.; Nestler, B.; Stinner, B. (2004): A diffuse interface model for alloys with multiple components and phases. *SIAM J. APPL. MATH*, vol. 64, no. 3, pp. 775–799.

Garcke, H.; Nestler, B.; Stoth, B. (1999): A multiphase field concept: Numerical simulations of moving phase boundaries and multiple junctions. *SIAM J. Appl. Math.*, vol. 60, no. 1, pp. 295–315.

Garcke, H.; Rumpf, M.; Weikard, U. (2001): The cahn-hilliard equaiton with elasticity-finite element approximation and qualitative studies. *Interfaces and Free Boundaries*, vol. 3, pp. 101–118.

Kim, J. (2002): *Modeling and simulation of multicomponent, multi-phase fluid flows*. PhD thesis, University of Minnesota, 2002.

Kim, J.; Kang, K.; Lowengrub, J. (2004): Conservative multigrid methods for cahn-hilliard fluids. *J. Comp. Phys.*, vol. 193, pp. 511–543.

Kim, J.; Kang, K.; Lowengrub, J. (2004): Conservative multigrid methods for ternary cahn-hilliard systems. *Comm. Math. Sci.*, vol. 2, no. 1, pp. 53–77.

Leo, P. H.; Lowengrub, J. S.; Jou, H. J. (1998): A diffuse interface model for microstructural evolution in elastically stressed solids. *Acta Mater.*, vol. 46, no. 6, pp. 2113–2130.

Nabarro, F. R. N.; Cress, C. M.; Kotschy, P. (1996): The thermodynamic driving force for rafting in superalloys. *Acta Mater.*, vol. 44, pp. 3189–3198.

Rozvany, G. (1989): *Structural Design via Optimality Criteria*. Dordrecht: Kluwer.

Sigmund, O. (2001): A 99 line topology optimization code written in matlab. *Structural and Multidisciplinary Optimization*, vol. 21, pp. 120–127.

Svanberg, K. (1987): The method of moving asymptotes-a new method for structural optimization. *International Journal for Numerical Methods in Engineering*, vol. 24, pp. 359–373.

Tang, P. S.; Chang, K. H. (2001): Integration of topology and shape optimization for design of structural components. *Structural and Multidisciplinary Optimization*, vol. 22, no. 1, pp. 65–82.

Zhou, S. W.; Wang, M. Y. (2005): The optimization of multi-material structure topology with cahn-hilliard model. *Structural and Multidisciplinary Optimization*, vol. accepted.

Appendix A: Proof of Non-Increasing Total Free Energy

The difference of the total energy after one iteration can be simplified as Eq. (29), which is derived from integral by part and the approximation of $\Delta c^{n+1/2} = (\Delta c^{n+1} + \Delta c^n)/2$ and $\mu^{n+1/2} = \hat{f}(c^{n+1}, c^n) - \Delta c^{n+1/2} + \hat{w}(c^{n+1}, \varepsilon^{n+1}, c^n, \varepsilon^n)$.

$$
\begin{aligned}
&\Psi\left(c^{n+1}\right) - \Psi\left(c^n\right) \\
&\quad = \int F\left(c^{n+1}\right) - F\left(c^n\right) \\
&\quad + \frac{\Gamma_\varepsilon}{2} \int \left(\nabla c^{n+1} \cdot \nabla c^{n+1} - \nabla c^n \cdot \nabla c^n\right) \\
&\quad + W^*(c^{n+1}, \varepsilon^{n+1}) - W^*(c^n, \varepsilon^n) \\
&\quad = \int \left[F\left(c^{n+1}\right) - F\left(c^n\right)\right] \\
&\quad + \frac{\Gamma_\varepsilon}{2} \int \left(\nabla c^{n+1} + \nabla c^n\right) \cdot \left(\nabla c^{n+1} - \nabla c^n\right)
\end{aligned}
$$

$$
\begin{aligned}
&+W^*(c^{n+1},\varepsilon^{n+1})-W^*(c^n,\varepsilon^n)\\
&=\int\left[F\left(c^{n+1}\right)-F\left(c^n\right)\right]\\
&-\int\Gamma_\varepsilon\frac{\left(\Delta c^{n+1}+\Delta c^n\right)}{2}\cdot\overline{c}\\
&+W^*(c^{n+1},\varepsilon^{n+1})-W^*(c^n,\varepsilon^n)\\
&=\int\left[F\left(c^{n+1}\right)-F\left(c^n\right)\right]\\
&+\int(\mu^{n+1/2}-\hat{f}(c^{n+1},c^n))\cdot\overline{c}\\
&-\int(\hat{w}(c^{n+1},\varepsilon^{n+1},c^n,\varepsilon^n))\cdot\overline{c}\\
&+W^*\left(c^{n+1},\varepsilon^{n+1}\right)-W^*\left(c^n,\varepsilon^n\right)\\
&=\int\left[F\left(c^{n+1}\right)-F\left(c^n\right)\right]-\int\hat{f}(c^{n+1},c^n)\cdot\overline{c}\\
&-\tau\int\left(\nabla\mu^{n+1/2}\right)^2-\int\hat{w}(c^{n+1},\varepsilon^{n+1},c^n,\varepsilon^n)\cdot\overline{c}\\
&+W^*\left(c^{n+1},\varepsilon^{n+1}\right)-W^*\left(c^n,\varepsilon^n\right)
\end{aligned}
\tag{29}
$$

Substitute Eqs. (25)-(27) to the second item in Eq. (29), get

$$
\begin{aligned}
&\hat{f}(c^{n+1},c^n)\cdot\overline{c}\\
&=f\left(c^{n+1}\right)\cdot\overline{c}-\frac{1}{2!}\overline{c}\nabla f\left(c^{n+1}\right)\cdot\overline{c}\\
&+\frac{1}{3!}\begin{bmatrix}\overline{c}^TH\left(f_1\left(c^{n+1}\right)\right)\cdot\overline{c}\\ \overline{c}^TH\left(f_2\left(c^{n+1}\right)\right)\cdot\overline{c}\\ \overline{c}^TH\left(f_3\left(c^{n+1}\right)\right)\cdot\overline{c}\end{bmatrix}\cdot\overline{c}
\end{aligned}
\tag{30}
$$

Extend the elastic part also with Taylor series and assure equilibrium deformation resulting in $\frac{\partial W^*(c^n,\varepsilon^n)}{\partial\varepsilon}=0$, get

$$
\begin{aligned}
&W^*\left(c^{n+1},\varepsilon^{n+1}\right)=W^*\left(c^n,\varepsilon^n\right)\\
&+\frac{\partial W^*\left(c^n,\varepsilon^n\right)}{\partial c}\cdot\overline{c}+\frac{1}{2}\frac{\partial W^{*2}\left(c^n,\varepsilon^n\right)}{\partial c^2}\cdot\overline{c}^2
\end{aligned}
\tag{31}
$$

Extend the derivative of elastic energy in Eq. (31)

$$
\begin{aligned}
&\hat{w}(c^{n+1},\varepsilon^{n+1},c^n,\varepsilon^n)\\
&=w\left(c^n,\varepsilon^n\right)+\frac{\partial w\left(c^n,\varepsilon^n\right)}{\partial c}\overline{c}
\end{aligned}
\tag{32}
$$

Expand $F(c^n)$ at $F(c^{n+1})$ according to Taylor series:

$$
\begin{aligned}
&F(c^n)=F(c^{n+1})-\overline{c}\cdot\frac{\partial F(c^{n+1})}{\partial c}\\
&+\frac{1}{2!}[\sum_{i=1}^{3}((c_i^{n+1}-c_i^n)\cdot\frac{\partial}{\partial c_i})]^2F(c^{n+1})\\
&-\frac{1}{3!}[\sum_{i=1}^{3}((c_i^{n+1}-c_i^n)\cdot\frac{\partial}{\partial c_i})]^3F(c^{n+1})\\
&+\frac{1}{4!}[\sum_{i=1}^{3}((c_i^{n+1}-c_i^n)\cdot\frac{\partial}{\partial c_i})]^4F(c^{n+1})\\
&\Longrightarrow F(c^{n+1})-F(c^n)\\
&=\nabla F\left(c^{n+1}\right)\cdot\overline{c}-\frac{1}{2!}\overline{c}H\left[F\left(c^{n+1}\right)\right]\cdot\overline{c}\\
&+\frac{1}{3!}\begin{bmatrix}\overline{c}H\left(f_1\left(c^{n+1}\right)\right)\cdot\overline{c}\\ \overline{c}H\left(f_2\left(c^{n+1}\right)\right)\cdot\overline{c}\\ \overline{c}H\left(f_3\left(c^{n+1}\right)\right)\cdot\overline{c}\end{bmatrix}\cdot\overline{c}\\
&-\frac{1}{4!}[\sum_{i=1}^{3}((c_i^{n+1}-c_i^n)\cdot\frac{\partial}{\partial c_i})]^4F(c^{n+1})
\end{aligned}
\tag{33}
$$

Put Eqs. (30)-(33) back to Eq. (29), get

$$
\begin{aligned}
&\Psi\left(c^{n+1}\right)-\Psi\left(c^n\right)\\
&=-\frac{1}{4!}[\sum_{i=1}^{3}((c_i^{n+1}-c_i^n)\cdot\frac{\partial}{\partial c_i})]^4F(c^{n+1})\\
&-\tau\int\left(\nabla\mu^{n+1/2}\right)^2-\frac{1}{2}\int\frac{\partial w\left(c^n,u^n\right)}{\partial c}\cdot\overline{c}^2
\end{aligned}
\tag{34}
$$

From the first derivative of elastic energy introduce by adjoint method [Bendsoe and Sigmund (2003)], $\frac{\partial W(c^n,\varepsilon^n)}{\partial c}=-pc^{p-1}u_eK_eu_e$, it is easy to get:

$$
\frac{\partial w\left(c^n,\varepsilon^n\right)}{\partial c}=\begin{cases}0 & if\ p=1\\ Pu_eK_eu_e\geq 0 & if\ p\geq 2\end{cases}
\tag{35}
$$

where $P=p(p-1)c^{p-2}$

According to the bulk function in Eq. (19) and the unit summation constraint for design variables c, it is directly to derive

$$
\begin{aligned}
&\frac{1}{4!}[\sum_{i=1}^{3}((c_i^{n+1}-c_i^n)\cdot\frac{\partial}{\partial c_i})]^4F(c^{n+1})\\
&=\frac{\kappa}{4!}[\frac{\partial F(c_{n+1})^4}{\partial^4\alpha}\overline{\alpha}^4+\frac{\partial F(c_{n+1})^4}{\partial^4\beta}\overline{\beta}^4\\
&+\frac{\partial F(c_{n+1})^4}{\partial^4\gamma}\overline{\gamma}^4+4\frac{\partial F(c_{n+1})^4}{\partial^3\alpha\partial\beta}\overline{\alpha}^3\overline{\beta}\\
&+4\frac{\partial F(c_{n+1})^4}{\partial^3\alpha\partial\gamma}\overline{\alpha}^3\overline{\gamma}+4\frac{\partial F(c_{n+1})^4}{\partial^3\beta\partial\alpha}\overline{\beta}^3\overline{\alpha}
\end{aligned}
$$

$$
\begin{aligned}
&+4\frac{\partial F(c_{n+1})^4}{\partial^3\beta\partial\gamma}\overline{\beta}^3\overline{\gamma}+4\frac{\partial F(c_{n+1})^4}{\partial^3\gamma\partial\alpha}\overline{\gamma}^3\overline{\alpha}\\
&+4\frac{\partial F(c_{n+1})^4}{\partial^3\gamma\partial\beta}\overline{\gamma}^3\overline{\beta}+6\frac{\partial F(c_{n+1})^4}{\partial^2\alpha\partial^2\beta}\overline{\alpha}^2\overline{\beta}^2\\
&+6\frac{\partial F(c_{n+1})^4}{\partial^2\alpha\partial^2\gamma}\overline{\alpha}^2\overline{\gamma}^2+6\frac{\partial F(c_{n+1})^4}{\partial^2\beta\partial^2\gamma}\overline{\beta}^2\overline{\gamma}^2\\
&+12\frac{\partial F(c_{n+1})^4}{\partial\alpha\partial\beta\partial^2\gamma}\overline{\alpha}\overline{\beta}\overline{\gamma}^2+12\frac{\partial F(c_{n+1})^4}{\partial\alpha\partial\gamma\partial^2\beta}\overline{\alpha}\overline{\gamma}\overline{\beta}^2\\
&+12\frac{\partial F(c_{n+1})^4}{\partial\beta\partial\gamma\partial^2\alpha}\overline{\beta}\overline{\gamma}\overline{\alpha}^2]\\
&=R_1+R_2
\end{aligned}
\tag{36}
$$

Where R_1 is the extension for the first part of bulk function $F_1=\kappa[\alpha^2(\beta^2+\gamma^2+\nu^2)+\beta^2(\gamma^2+\nu^2)+\gamma^2\nu^2]$. It is equal to:

$$
\begin{aligned}
R_1&=\kappa(\overline{\alpha}^4+\overline{\beta}^4+\overline{\gamma}^4+2\overline{\alpha}^3\overline{\beta}+2\overline{\alpha}^3\overline{\gamma}\\
&+2\overline{\beta}^3\overline{\alpha}+2\overline{\beta}^3\overline{\gamma}+2\overline{\gamma}^3\overline{\alpha}+2\overline{\gamma}^3\overline{\beta}+3\overline{\alpha}^2\overline{\beta}^2\\
&+3\overline{\alpha}^2\overline{\gamma}^2+3\overline{\beta}^2\overline{\gamma}^2+2\overline{\beta}\overline{\gamma}\overline{\alpha}^2+2\overline{\alpha}\overline{\gamma}\overline{\beta}^2+2\overline{\alpha}\overline{\beta}\overline{\gamma}^2)\\
&=\kappa[(\overline{\alpha}^2+\overline{\beta}^2+\overline{\gamma}^2)(\overline{\alpha}+\overline{\beta}+\overline{\gamma})^2\\
&+\overline{\alpha}^2\overline{\beta}^2+\overline{\alpha}^2\overline{\gamma}^2+\overline{\beta}^2\overline{\gamma}^2]\geq 0
\end{aligned}
\tag{37}
$$

R_2 is the one for the rest part of bulk function $F_2=\kappa[\alpha^2\beta^2(\gamma^2+\nu^2)+\beta^2\gamma^2\nu^2]$. We can prove all coefficients for R_1+R_2 are greater than the ones for $C_{min}R_1$ by expanding $1=(\alpha+\beta+\gamma+\nu)^2$ as following:

$$
\begin{aligned}
&T_1+S_1=(1+\beta^2)\geq C_{min}T_1\\
&T_2+S_2=(1+(\alpha^2+\gamma^2)\geq C_{min}T_2\\
&T_3+S_3=(1+\beta^2)\geq C_{min}T_3\\
&T_4+S_4=(2+(-4\beta\nu+2\beta^2+4\alpha\beta))\geq C_{min}T_4\\
&T_5+S_5=(2+2\beta^2)\geq C_{min}T_5\\
&T_6+S_6=(2+(-4\alpha\nu+2\alpha^2+4\alpha\beta+2\gamma^2))\geq C_{min}T_6\\
&T_7+S_7=(2+(2\alpha^2-4\gamma\nu+2\gamma^2+4\beta\gamma))\geq C_{min}T_7\\
&T_8+S_8=(2+2\beta^2)\geq C_{min}T_8\\
&T_9+S_9\\
&=3+(2\gamma^2+\nu^2-4\beta\nu+\beta^2-4\alpha\nu+8\alpha\beta+\alpha^2)\\
&\geq C_{min}T_9\\
&T_{10}+S_{10}=(3+3\beta^2)\geq C_{min}T_{10}\\
&T_{11}+S_{11}\\
&=3+(2\alpha^2+\nu^2-4\gamma\nu+\gamma^2-4\beta\nu+8\beta\gamma+\beta^2)\\
&\geq C_{min}T_{11}\\
&T_{12}+S_{12}=(2+(2\beta(2\gamma-2\nu)+2\beta^2+8\alpha\beta+4\beta\gamma))\\
&\geq C_{min}T_{12}\\
&T_{13}+S_{13}\\
&=2+(4\alpha(\gamma-\nu)+2\alpha^2+8\alpha\beta-4\gamma\nu+2\gamma^2+8\beta\gamma)\\
&\geq C_{min}T_{13}\\
&T_{14}+S_{14}=(2+(8\alpha\beta-4\beta\nu+2\beta^2+8\beta\gamma))\geq C_{min}T_{14}
\end{aligned}
\tag{38}
$$

Where T_i and S_i are the coefficients for $\overline{\alpha}^i\overline{\beta}^j\overline{\gamma}^k, i\geq 0, j\geq 0, k\geq 0, i+j+k=4$ in R_1 and R_2 respectively. C_{min} is a positive constant. We also use α to represent α^{n+1} for brief reason. Thus, it is easy to derive:

$$
\begin{aligned}
&\frac{1}{4!}[\sum_{i=1}^{3}((c_i^{n+1}-c_i^n)\cdot\frac{\partial}{\partial c_i})]^4F(c^{n+1})\\
&=R_1+R_2\geq C_{min}R_1\geq 0
\end{aligned}
\tag{39}
$$

Eqs. (34), (35) and (39) indicate the total free energy is a Lyapunov functional without minimal time step restriction.

$$
\Psi\left(c^{n+1}\right)-\Psi\left(c^n\right)\leq 0 \tag{40}
$$

Appendix B: Proof of Convergence

The approximation in Eqs. (25)-(27) also leads to:

$$
\begin{aligned}
&\left|f\left(\frac{c^n+c^{n+1}}{2}\right)-\hat{f}\left(c^n,c^{n+1}\right)\right|\\
&\leq C\left|c^{n+1}-c^{n+1}\right|^2
\end{aligned}
\tag{41}
$$

which is a prerequisite for the convergence of this algorithm within fixed time step. To prove Eq. (41), we first discretize $f_1\left(\frac{c^n+c^{n+1}}{2}\right)=f_1\left(c^{n+1}+\frac{c^n-c^{n+1}}{2}\right)$ at c^{m+1} by Taylor series:

$$
\begin{aligned}
&f_1\left(\frac{c^{n+1}+c^n}{2}\right)\\
&=f_1\left(c^{n+1}\right)+\nabla f_1\left(c^{n+1}\right)\cdot\left(\frac{c^n-c^{n+1}}{2}\right)\\
&+\frac{1}{2!}\left(\frac{c^n-c^{n+1}}{2}\right)\nabla f_1\left(c^{n+1}\right)\cdot\left(\frac{c^n-c^{n+1}}{2}\right)
\end{aligned}
\tag{42}
$$

then,

$$
\begin{aligned}
&f_1\left(\frac{c^{n+1}+c^n}{2}\right)-\hat{f}_1\left(c^n,c^{n+1}\right)\\
&\quad=-\frac{1}{24}\overline{c}^T H\left(f_1\left(c^n\right)\right)\cdot\overline{c}\\
&\quad=-\frac{1}{24}\frac{\partial^2 f_1\left(c^{n+1}\right)}{\partial\alpha^2}\overline{\alpha}^2-\frac{1}{24}\frac{\partial^2 f_1\left(c^{n+1}\right)}{\partial\beta^2}\overline{\beta}^2\\
&\quad-\frac{1}{24}\frac{\partial^2 f_1\left(c^{n+1}\right)}{\partial\gamma^2}\overline{\gamma}^2-\frac{1}{12}\frac{\partial^2 f_1\left(c^{n+1}\right)}{\partial\alpha\partial\beta}\overline{\alpha}\overline{\beta}\\
&\quad-\frac{1}{12}\frac{\partial^2 f_1\left(c^{n+1}\right)}{\partial\alpha\partial\gamma}\overline{\alpha\gamma}-\frac{1}{12}\frac{\partial^2 f_1\left(c^{n+1}\right)}{\partial\beta\partial\gamma}\overline{\beta}\overline{\gamma}
\end{aligned}
\tag{43}
$$

Applying Young's inequality to Eq. (43) and considering the bound of f_1 and its derivative in the first/second order, we get

$$
\begin{aligned}
&\left|f_1\left(\frac{c^{n+1}+c^n}{2}\right)-\hat{f}_1\left(c^n,c^{n+1}\right)\right|\\
&\quad\le C(\overline{\alpha}^2+\overline{\beta}^2+\overline{\gamma}^2)
\end{aligned}
\tag{44}
$$

where C is a constant. Similarly, we get

$$
\begin{aligned}
&\left|f_2\left(\frac{c^{n+1}+c^n}{2}\right)-\hat{f}_2\left(c^n,c^{n+1}\right)\right|\\
&\quad\le C(\overline{\alpha}^2+\overline{\beta}^2+\overline{\gamma}^2)
\end{aligned}
\tag{45}
$$

$$
\begin{aligned}
&\left|f_3\left(\frac{c^{n+1}+c^n}{2}\right)-\hat{f}_3\left(c^n,c^{n+1}\right)\right|\\
&\quad\le C(\overline{\alpha}^2+\overline{\beta}^2+\overline{\gamma}^2)
\end{aligned}
\tag{46}
$$

Finally get,

$$
\begin{aligned}
&\left|f\left(\frac{c^n+c^{n+1}}{2}\right)-\hat{f}\left(c^n,c^{n+1}\right)\right|\\
&\quad\le C\left|c^{n+1}-c^n\right|^2
\end{aligned}
\tag{47}
$$

from Eq. (47), it is easy to prove [Kim, Kang, and Lowengrub (2004a)] the convergence of the algorithm within fixed time step.

$$
\left\|u^n-c^n\right\|\le C\left(h^2+\tau^2\right) \tag{48}
$$

where u^n is the smooth solution.